THE JOURNAL OF PHYSICAL CHEMISTRY C

Article

pubs.acs.org/JPCC

Porphyrin Nanocrystal Synthesized via Chemical Reaction Route: pH-Sensitive Reversible Transformation between Nanocrystals and Bulk Single Crystal

Liang Wang,[†] Yanli Chen,[‡] Yongzhong Bian,[†] and Jianzhuang Jiang*[,†]

[†]Beijing Key Laboratory for Science and Application of Functional Molecular and Crystalline Materials, Department of Chemistry, University of Science and Technology Beijing, Beijing 100083, China

[‡]Department of Chemistry, University of Jinan, Jinan 250022, China

Supporting Information

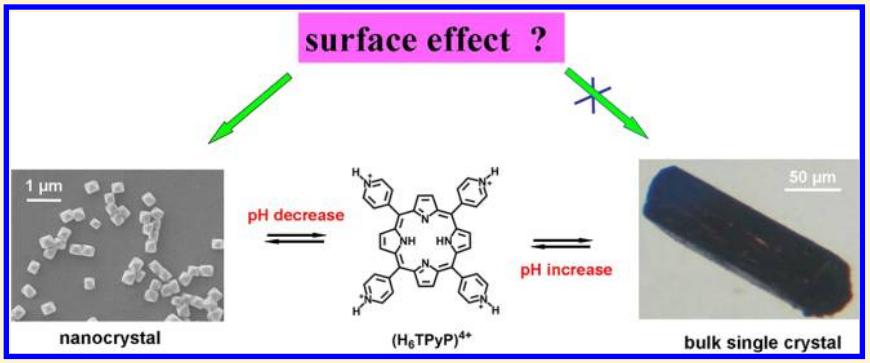

ABSTRACT: Crystalline nanostructures with octahedral morphology have been prepared by self-assembling of cationic porphyrin $(H_6TPyP)^{4+}\cdot 4Cl^-$ produced through chemical reaction route in aqueous solution depending on the synergistic interactions among hydrogen-bonding, $\pi-\pi$ stacking, and ion pairing. Unexpectedly, the gradual decrease in pH by the slow evaporation of solvent in the nano-octahedron aqueous suspension obtained in situ led to the selective etching of the original nanocrystal and the isolation of $(H_6TPyP)^{4+}\cdot 4Cl^-$ bulk single crystals in the last stage. More interestingly, the increase in pH by adding water again into this bulk single-crystal-containing system led to the regeneration of nano-octahedrons, indicating the reversible transformation between porphyrin nano-octahedrons and bulk single crystals triggered by pH. Mechanistic investigations through powder and single-crystal X-ray diffraction analyses together with the electron microscopic, in particular, HRTEM, clearly reveal that the unique surface effect and anisotropic character of the nanomaterials differing from the bulk organic materials are responsible for such pH-sensitive reversible transformation of the two crystalline materials by controlling the dissolution or aggregation of $(H_6TPyP)^{4+}\cdot 4Cl^-$, which actually induces the reversible formation and breaking of the (pyridine)N^+–H···Cl^-···H–O(H_2O)···H–N^+(pyridine) hydrogen bonds among cationic porphyrin building blocks at different pH. This result, to control the crystallinity and the unprecedented reversible transformation between nanocrystal and bulk single crystals just by tuning the pH of the synthesis process, as well as the use of the peculiar nanoeffect such as surface effect to adjust the self-assembling process, provides useful a tool for the controllable synthesis of crystalline materials and is expected to be helpful for further research and application of organic nanomaterials.

INTRODUCTION

Because of their potential applications in catalysis, optical device, storage, field-effect transistor and photovoltaics self-assembling of functional organic molecules into well-defined nanostructures ranging from nanospheres, nanotubes, to nanofibers has been the focus of material science and technology.[1−3] In particular, the nanocrystals have gotten much more attention due to their long-range order of molecular arrangement.[4−8] Various noncovalent interactions including $\pi-\pi$ interaction, van der Waals, hydrogen bonding, hydrophilic/hydrophobic, electrostatic, and metal−ligand coordination act as the driving force in the self-assembling process,[9−11,14−23] among which the hydrogen bonding is particularly interesting because of its reversibility in response to the external stimulus such as pH and heating,[12,13] but until now, research on the stimulus-responding reversible structure transformation of nanomaterials based on hydrogen-bonding interaction is still rare,[12,13] although it is very interesting and challenging in nanoscience and nanotechnology.

As part of our continuous efforts toward the fabrication of ordered porphyrin-involved nanostructures with potential application in organic field effect transistor (OFET) devi-

Received: June 7, 2013
Revised: July 24, 2013
Published: July 30, 2013

   dx.doi.org/10.1021/jp4056544 | J. Phys. Chem. C 2013, 117, 17352−17359

Scheme 1. Schematic Molecular Structures of H_2TPyP, $(H_8TPyP)^{6+}$, and $(H_6TPyP)^{4+}$ and the Chemical Reaction Route to Produce the Target Molecules

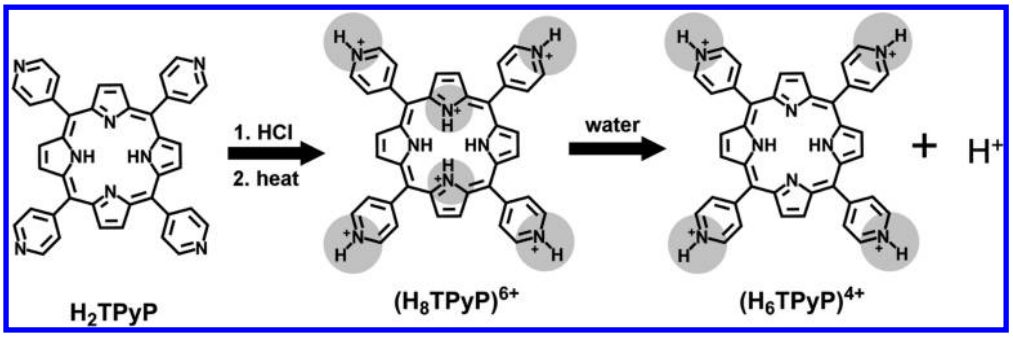

ces,[14−23] facile procedure toward crystalline nanostructures of H_2TPyP derivative was explored, leading to the easy preparation of crystalline nano-octahedrons through the self-assembly of cationic porphyrin $(H_6TPyP)^{4+}\cdot 4Cl^-$ produced through a chemical route in aqueous solution depending on the synergistic interactions among hydrogen-bonding, $\pi-\pi$ stacking, and ion-pairing, in which the separated nucleating and growth process in the chemical reaction route as well the proper pH contribute to the crystallization of the nanocrystals. Most importantly, because of the reversible formation and break of the (pyridine)$N^+-H\cdots Cl^-\cdots H-O(H_2O)\cdots H-N^+$(pyridine) hydrogen bonds involved among cationic porphyrin building blocks in response to the pH, the as-prepared uniformed nano-octahedrons selectively etched into hollow nano-octahedrons with the decrease in pH owing to the evaporation of solvent and bulk single crystals were obtained in the last stage. More interestingly, readdition of water into the suspension containing bulk single crystals resulted in the nanocrystals with octahedral morphology again. Mechanism investigation shows that surface effect and anisotropic character of the nanomaterials play a key role in such process. To the best of our knowledge, there is no report of such pH-triggered reversible transformation between these two organic crystalline materials prior to this work.

EXPERIMENTAL SECTION

Materials and Characterization. The tetrakis(4-pyridyl)-porphyrin (H_2TPyP) was purchased from J&K Scientific. All other reagents and solvents were of reagent grade and used as received. Electronic absorption spectra were recorded on a Hitachi U-4100 spectrophotometer. Powder X-ray diffraction (PXRD) data were collected on a Shimadzu XRD-6000 diffractometer using Cu-Ka radiation (l = 1.54056 Å) at room temperature. TEM images were measured on a JEOL JEM-2100 electron microscope operated at 200 kV. SEM images were obtained using a JEOL JEM-6510A scanning electron microscopy. For TEM and SEM imaging, a drop of freshly prepared sample solution was cast onto a carbon copper grid. For SEM imaging, gold (1 to 2 nm) was sputtered onto the grids to prevent charging effects and to improve the image clarity.

Preparation of $(H_6TPyP)^{4+}\cdot 4Cl^-$ Nanocrystals and Single Crystals. Typically, H_2TPyP (6 mg) was dissolved in hydrochloric acid (5 mL, 12 M), heated to 120 °C to dry, and kept at this temperature for a further 15 min. After being cooled to room temperature, 20 mL of water was added to redissolve the green solid, resulting in a red solution, which soon turned into a cloudy brown suspension system, centrifugation of which provided corresponding $(H_6TPyP)^{4+}\cdot 4Cl^-$ nano-octahedron with the edge length of ca. 250 nm. Keeping the nano-octahedron suspension system in water obtained in situ in air for several days ranging from 1 to 2 weeks after the evaporation of solvent led to the isolation of purple quadrangular $(H_6TPyP)^{4+}\cdot 4Cl^-$ single crystals. Adding water again to the above water-evaporated system led to a cloudy brown suspension system containing $(H_6TPyP)^{4+}\cdot 4Cl^-$ octahedral nanocrystals immediately again.

To further confirm the growth mechanism of single crystals of $(H_6TPyP)^{4+}\cdot 4Cl^-$, we put the freshly prepared suspension into a sealed container for the same period mentioned above to produce the bulk single crystal, but there was no bulk single crystal observed. In addition, the freshly prepared suspension containing the nanocrystals was filtrated. The filtrate was evaporated in air for several days, which provided few unknown precipitates. The filtrated nanocrystals were dispersed in 20 mL of water and evaporated in air for the same period, but no bulk single crystal was obtained either.

X-ray Crystallographic Analyses. Data were collected on an Oxford Diffraction Gemini E system with Cu Kα radiation λ = 1.5418 Å at 293 K using a ω-scan mode with an increment of 0.3°. Preliminary unit cell parameters were obtained from 30 frames. Final unit cell parameters were obtained by global refinements of reflections obtained from the integration of all of the frame data. The collected frames were integrated using the preliminary cell-orientation matrix. The SMART software was used for data collecting and processing;[24] ABSpack was used for absorption correction;[24] and SHELXL was used for space-group and structure determination, refinements, graphics, and structure reporting.[25] CCDC-910529 contains the supplementary crystallographic data for this paper. These data can be obtained free of charge from the Cambridge Crystallographic Data Centre via www.ccdc.cam.ac.uk/data_request/cif.

RESULTS AND DISCUSSION

Preparation of $(H_6TPyP)^{4+}\cdot 4Cl^-$ Nanocrystals with Octahedral Morphology and Bulk Single Crystals. To get crystalline nanomaterials, we employed the chemical reaction method[10] in which the target molecules were produced in situ gradually via chemical reaction route from precursor molecules. Thus the nucleation and growth stages were separated, which slows the growth speed of the nanostructures and also helps to avoid the broad distribution of the size and shape of the final product. In our experiment, H_2TPyP (Scheme 1) with four pyridine-N atoms at outer position and two pyrrol-N at the porphyrin core was selected as the precursor molecules, which are easily to be all or partially

dx.doi.org/10.1021/jp4056544 | J. Phys. Chem. C 2013, 117, 17352−17359

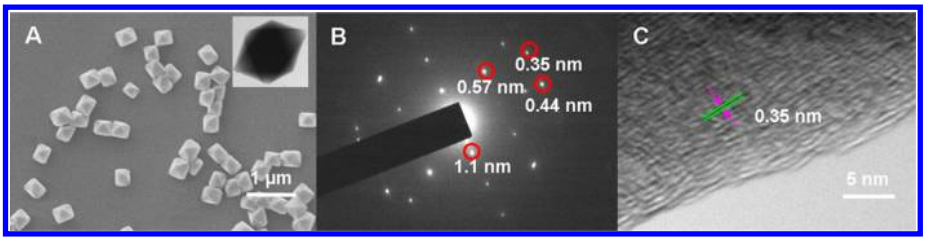

Figure 1. SEM images of the self-assembled $(H_6TPyP)^{4+}\cdot 4Cl^-$ nano-octahedron with the average edge length of 250 nm (with the inset showing the magnified TEM images of corresponding nanocrystals) (A), the SAED patterns taken from the individual nano-octahedron (B), and HRTEM image of individual nano-octahedron (C).

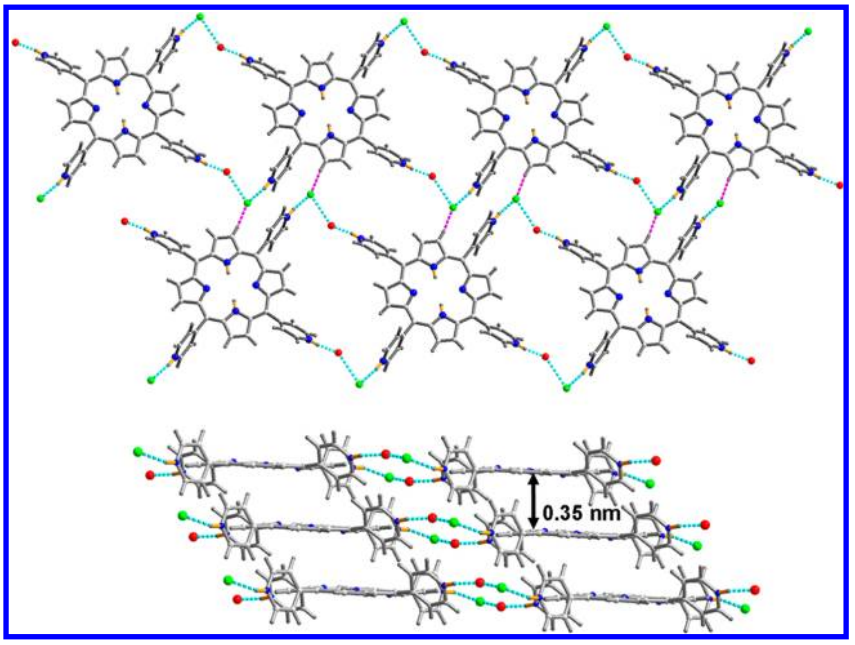

Figure 2. Crystal structure of $(H_6TPyP)^{4+}\cdot 4Cl^-$ in two perspective views (chloride: green; nitrogen: blue; H_2O: red; H: gray). Some solvent molecules are omitted for clarity.

protonated depending on the pH of the environment owing to the different basicity of the two kinds of nitrogen atoms and become pyridinium or pyrrol salt that can form hydrogen-bonded net works with each other at proper pH.[26] As detailed in the Experimental Section and Scheme 1, dissolution of H_2TPyP into excess condensed hydrochloric acid solution led to the production of $(H_8TPyP)^{6+}\cdot 6Cl^-$, which has four protonated pyridine-N atoms at the outer position and two protonated pyrrol-N atoms at the porphyrin core and is able to form aqueous solution owing to the large electrostatic repulsion between the $(H_8TPyP)^{6+}$ porphyrin cores. Evaporation of excess HCl, followed by redissolving the resulting residue in water, induces the gradual ionization from $(H_8TPyP)^{6+}\cdot 6Cl^-$ into $(H_6TPyP)^{4+}\cdot 4Cl^-$, in which four pyridine-N atoms at the outer position keep protonated while two pyrrol-N atoms at the porphyrin core are neutralized due to the different basicity of the two type of nitrogen atoms (Scheme 1). Synergistic noncovalent interactions among hydrogen bonding and $\pi-\pi$ interaction of $(H_6TPyP)^{4+}$ building blocks as well as the ion-pairing interaction due to the existence of Cl^- ions in water then led to the simultaneous formation of $(H_6TPyP)^{4+}\cdot 4Cl^-$ nanocrystals with octahedral morphology (Figure 1A), the distinct edges of which indicated the good crystallinity of the nano-octahedrons. In addition, as clearly shown in Figure 1, the bright selected area electronic diffraction (SAED) patterns observed for the nano-octahedrons also suggest the single-crystalline nature of these nanostructures (Figure 1B). This is confirmed by the good agreement in the *d* spacings revealed by the diffraction spots in the SAED diffraction patterns and those simulated according to single-crystal X-ray diffraction analysis result (vide infra). In addition, perfect layered arrangement of the porphyrin molecules in the nano-octahedrons with crystalline nature can also be clearly reflected by the distinct lattice fringes with interlattice spacing of 0.35 nm observed in their HRTEM image (Figure 1C).

Unexpectedly, evaporation of the solvent of the nano-octahedron suspension system in water obtained in situ for several days ranging from 1 to 2 weeks induces the formation and isolation of bulk single crystals of $(H_6TPyP)^{4+}\cdot 4Cl^-$, Figure S1 (Supporting Information). Interestingly, readdition of water into this $(H_6TPyP)^{4+}\cdot 4Cl^-$ bulk single-crystal-containing system results, again, in the production of $(H_6TPyP)^{4+}\cdot 4Cl^-$ octahedral nanocrystals. At the same time, the as-prepared bulk single crystals were dissolved. Such a novel reversible transformation between nanocrystals and bulk single crystals triggered just by evaporation or addition of solvent is particularly interesting, which attracted us to pursue the origin of such a reversible transformation.

Single-Crystal Structure. As summarized in Table S1 (Supporting Information), the cationic molecular porphyrin crystallizes in triclinic *P*-1 space group. The asymmetric unit consists of half $(H_6TPyP)^{4+}$ molecule, two chloride ions, and

dx.doi.org/10.1021/jp4056544 | J. Phys. Chem. C 2013, 117, 17352−17359

five water molecules. Figure S2 (Supporting Information) shows the molecular structure of $(H_6TPyP)^{4+}$ in the single crystal. The planar porphyrin molecular structure confirms the diproton instead of tetraproton nature of the central tetrapyrrole core.[14,27] As can be seen from the crystal-packing diagram of $(H_6TPyP)^{4+}\cdot 4Cl^-$ (Figure 2), each porphyrin molecule is bound to two neighboring porphyrin molecules via (pyridine)N^+–H···Cl^-···H–O(H_2O)···H–N^+ (pyridine) hydrogen bonds with the help of a Cl^- ion and a water molecule with the length of NH···Cl = 0.305 nm, OH···Cl = 0.308 nm, and NH···O = 0.264 nm, leading to a head-to-tail 1D linear porphyrin chain. This linear porphyrin chain is held together by C–H···Cl hydrogen bond with the length of CH···Cl = 0.366 nm between the pyrrole CH of one chain and the chloride ion of the neighboring chain, forming a 2D sheet-like porphyrin array. Furthermore, $\pi-\pi$ interactions between porphyrin chromophores in a neighboring layer of arrays provide additional linkage between adjacent layers in the crystal with the van der Waals void space between porphyrin rings of 0.35 nm (Figure 2), leading to the formation of a 3D multilayer lamellar structure for the single crystal of $(H_6TPyP)^{4+}\cdot 4Cl^-$.[17,19]

Electronic Absorption Spectra. To reveal the formation and growth mechanism of $(H_6TPyP)^{4+}\cdot 4Cl^-$ nano-octahedron, the whole preparation process was monitored via UV–visible spectroscopy. As exhibited in Figure 3a,b, after dissolving

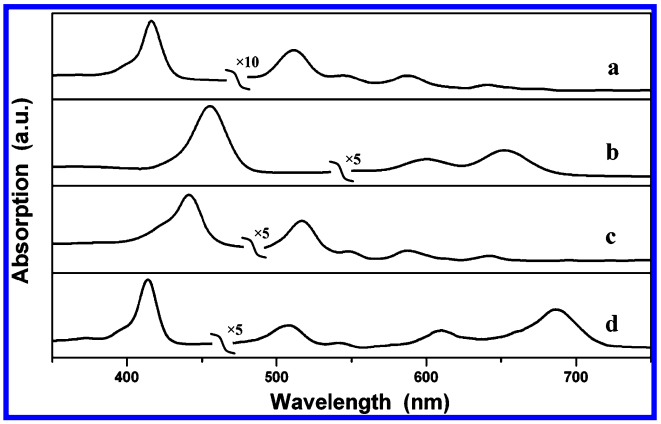

Figure 3. Electronic absorption spectra of (a) H_2TPyP in $CHCl_3$, (b) $(H_8TPyP)^{6+}$ in water obtained by dissolving H_2TPyP in hydrochloric acid, (c) $(H_6TPyP)^{4+}$ in water (actually the supernatant liquor of resulting system after removing nanocrystals by centrifugation), and (d) as-prepared nanocrystals dispersed in THF.

H_2TPyP in hydrochloric acid, typical features of a metal-free porphyrin with four weak Q absorption bands in the range of 500–700 nm disappeared and changes to two Q bands in the same area due to the increase in molecular symmetry from D_{2h} to D_{4h} indicated the formation of protonated $(H_8TPyP)^{6+}$,[26,28] which can also be confirmed by appearance of the green solution, typically indicating the protonation of porphyrin core. The red shift and broadening in both the porphyrin Soret and Q bands of $(H_8TPyP)^{6+}$ compared with expected ones are obviously associated with the formation of corresponding J-type aggregates of the latter species[16,18] between the neighboring cationic porphyrin molecules.[24] Further evaporating excess hydrochloric acid followed by redissolving the residue into water induces the formation of nano-octahedrons immediately depending on the synergetic interactions among hydrogen bonding, ion-pairing, and $\pi-\pi$ stacking. During this process, the four Q-bands of typical electronic absorption spectroscopic feature of free porphyrin with D_{2h} molecular symmetry were reobtained for both solution and nanocrystal samples, Figure 3c,d, which as well as the red-brown nanocrystal suspension all indicated the production of free base $(H_6TPyP)^{4+}$ from acidified $(H_8TPyP)^{6+}$ species via chemical reaction route. In addition, the S-band of the nanocrystal blue-shifted in comparison with the free $(H_6TPyP)^{4+}\cdot 4Cl^-$ molecule in solution, indicating the formation of *H*-type aggregation in the nanocrystals via intense $\pi-\pi$ stacking between the two porphyrin cores, which is also in agreement with the X-ray single-crystal analysis.

The above UV–visible spectroscopic tracing fully confirmed the formation process of the nanocrystals via chemical reaction route, as shown in Scheme 1, in which the step of producing the cationic porphyrin H_6TPyP^{4+} is the key stage because it controlled the aggregation speed of the H_6TPyP^{4+} and finally the crystallinity of the nano-octahedrons. It is well known that the rapid growth speed of the nanostructures often leads to the production of amorphous nanomaterials rather than crystalline materials. In our experiment, the $(H_6TPyP)^{4+}\cdot 4Cl^-$ molecules were produced gradually, and the molecules aggregated when nearly reaching the thermodynamic equilibrium, which leads to the production of nanocrystals. In addition, the H^+ from the residue HCl after the evaporation of excess hydrochloric acid may also contribute to the formation of the crystalline nano-octahedrons by reducing the aggregation speed. Because hydrogen bond is sensitive to the pH, when the pH is low enough the hydrogen bond will break.[29,30] As a result, the existence of residue HCl will slow the formation speed of the hydrogen bond among the cationic porphyrin $(H_6TPyP)^{4+}\cdot 4Cl^-$, which eventually helps the production of nanocrystals. Such a result may provide a facile way for the preparation of crystalline nanomaterials based on hydrogen-bonding interaction.

Powder X-ray Diffraction Analysis. The internal structure of $(H_6TPyP)^{4+}\cdot 4Cl^-$ nanocrystals was investigated by powder X-ray diffraction analysis. As shown in Figure 4a, the XRD pattern of the $(H_6TPyP)^{4+}\cdot 4Cl^-$ nanostructures fully agrees with that simulated according to the single-crystal X-ray

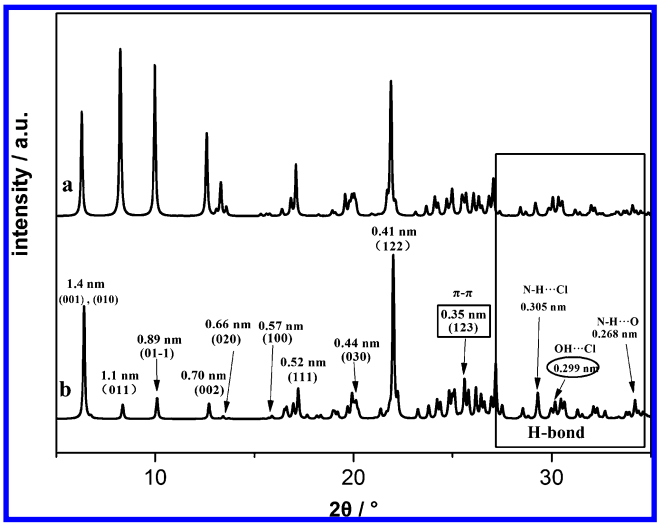

Figure 4. X-ray diffraction pattern of the $(H_6TPyP)^{4+}\cdot 4Cl^-$ nanocrystals (a) and the simulated pattern obtained according to the single crystal X-ray diffraction data (b).

dx.doi.org/10.1021/jp4056544 | J. Phys. Chem. C 2013, 117, 17352–17359

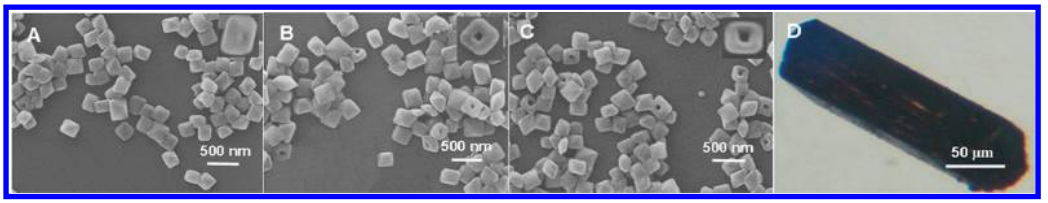

Figure 5. Evolution process of the $(H_6TPyP)^{4+}\cdot 4Cl^-$ nanocrystals with the edge of 250 nm observed by SEM after evaporation of water in air for 5 days (A), 9 days (B), and 12 days (C) with the inset pictures showing the magnified SEM images of representative etched nanocrystal in different stages. (D) Bulk single crystal coexisting with the nanocrystal, as shown in panel C.

data using the Mercury 2.2 program, except for the relative difference in the intensities of corresponding diffractions due to the different periodic unit number between nanocrystals and single crystals (Figure 4b). This result demonstrates the high purity of the bulk phase of $(H_6TPyP)^{4+}\cdot 4Cl^-$ nano-octhedrals and, in particular, the complete same internal structure between nanocrystals and single crystal of $(H_6TPyP)^{4+}\cdot 4Cl^-$.

pH-Sensitive Reversible Transformation Process between $(H_6TPyP)^{4+}\cdot 4Cl^-$ Nanocrystals and Bulk Single Crystals. Bulk organic single crystals play a key role in determining the internal structure of the organic materials on the basis of the single-crystal X-ray diffraction analysis, while the internal structure determined the functional performance of the materials. Conventionally, the organic single crystals grow slowly in a homogeneous solution by diffusion of poor solvent into the good solvent or by slow evaporation of the good solvent,[14,31−33] while in our experiment the single crystals grew in a suspension in which the nanostructures dispersed in poor solvent, which indeed is a very interesting phenomenon. To the best of our knowledge, there is still no such report prior to the present work.

For the purpose of elucidating the formation mechanism of the bulk single crystals of $(H_6TPyP)^{4+}\cdot 4Cl^-$ from the nanocrystal, the evolution process of the $(H_6TPyP)^{4+}\cdot 4Cl^-$ nanocrystals during the evaporation of water in the nanocrystal suspension system was monitored using SEM technique until the observation of bulk single crystals. Figure 5 displayed the SEM tracing images of the $(H_6TPyP)^{4+}\cdot 4Cl^-$ nanocrystals with the edge length of 250 nm observed after evaporation of water in air for 5, 9, and 12 days, respectively, which indicated that the octahedral nanocrystals were etched gradually and some formed hollow structures in different stages. At the beginning, without the evaporation of solvent, the nanostructures were perfect octahedron with smooth surface and distinct edges, and the pH of the suspension was 2.5 (Figure 1B). It is should be noted that the color of the suspension is red-brown. Along with the evaporation of the water, the volume as well as the pH of the suspension reduced. After 5 days, the pH became 2.2 and the edges of the nanocrystal became blunt and the surfaces became rough (Figure 5A). Meanwhile two vertices of nano-octahedrons were etched deeper and led to the formation of small shallow holes, as shown in the magnified image in Figure 5A. Notably, the holes appeared only at the two opposite vertices of octahedral nanocrystals, and the other four vertices remained unchanged, suggesting the different molecule arrangement at different vertices. After 9 days, the holes became deeper and the nano-octahedrons actually became a hollow tetragonal plate due to the disappearance of two vertices at the opposite positions, which also indicated the faster etching speed along this direction than the other two vertical directions. At the same time, the number of the vertices-etched nano-octahedrons became more (Figure 5B). In addition, the pH of suspension lowered to 1.9, and the color became light-brown. After 2 weeks, only a little water with dark-brown color remained, and the pH of the suspension became 1.5. At the same time, light-brown crystals suitable for single-crystal analysis were obtained (Figure 5D). SEM images showed that the hole in the hollow tetragonal plate became larger and fragments appeared in the remaining nanostructures (Figure 5C), indicating that some hollow tetragon plates were destroyed and the growing process of the bulk single crystals occurred on depletion of the nanocrystals.

The selective etching of the nanocrystal, as revealed by the above SEM tracing experiment and the color of the suspension getting deeper with the evaporation of water, clearly indicated that the concentration of $(H_6TPyP)^{4+}\cdot 4Cl^-$ increased in the process, which finally led to the growth of the bulk single crystal when the concentration reached saturation. To further confirm the conclusion, additional contrast experiments were carried out. First, nanocrystals in the suspension obtained in situ remained unchanged when being stored in a sealed container for the same period, indicating the important role of solvent evaporation for the formation of $(H_6TPyP)^{4+}\cdot 4Cl^-$ single crystal. Second, the nanocrystals were separated from the suspension by filtration and dispersed in water again. The filtrate was then put in air for evaporation, generating little unknown precipitate after several days, indicating that the dissolved $(H_6TPyP)^{4+}\cdot 4Cl^-$ in original suspension is not enough to grow into bulk single crystals. Similarly, even complete evaporation of the solvent in the system obtained by dispersing the obtained nanocrystal into the same volume of water as filtrate in air led to no porphyrin bulk single crystal either, which indicates the key role of the pH value, actually the residue H^+ on the formation of bulk single crystals.

As a consequence, the decrease in pH due to the increase in the concentration of H^+ with the evaporation of water finally led to the selective etching of the nanocrystals due to the break of hydrogen-bond networks. When the concentration of free $(H_6TPyP)^{4+}\cdot 4Cl^-$ reached saturation, bulk single crystals were produced. Obviously, the pH plays a key role in the formation of bulk single crystals by controlling the break of the hydrogen bond.

Interestingly, when water was added to the bulk single crystal containing suspension obtained by the gradual evaporation of water, the large single crystals dissolved and the nano-octahedrons formed again, as evidenced by the SEM images in Figure S3 (Supporting Information). It is worth noting that the pH of the suspension returned to 2.5 again, indicating that the bulk single crystals are not stable in higher pH. This further confirmed the pH-sensitive nature of the hydrogen-bonding-involved organic materials. In addition, the etched nanostructures also returned to the original nano-octahedrons with distinct edges.

dx.doi.org/10.1021/jp4056544 | J. Phys. Chem. C 2013, 117, 17352−17359

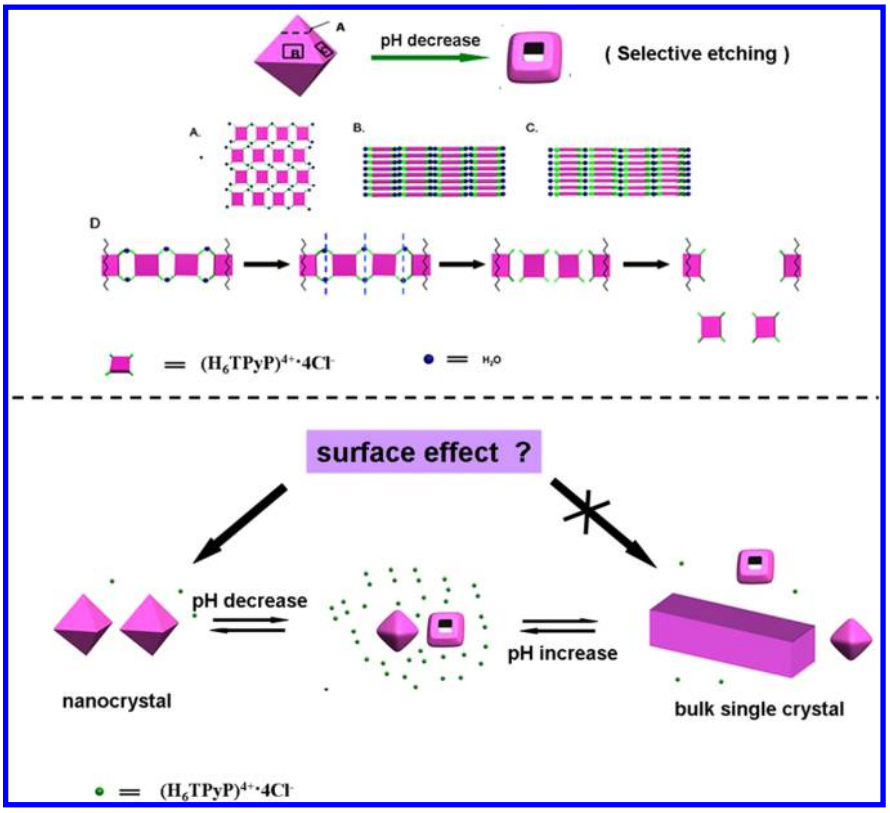

Figure 6. Schematic illustration of mechanism for selective etching of $(H_6TPyP)^{4+}\cdot 4Cl^-$ nano-octahedrons (upper field) and the reversible transformation between nanocrystals and bulk single crystal (lower field). (A–C) Molecule packing of corresponding cross section along different direction. (D) Break process of the hydrogen bond during the etching of the nanocrystals.

Mechanism of pH Sensitive Reversible Transformation between $(H_6TPyP)^{4+}\cdot 4Cl^-$ Nanocrystals and Single Crystals. From the above discussion, the control of pH induced the selective etching and finally the reversible transformation between $(H_6TPyP)^{4+}\cdot 4Cl^-$ nanocrystals and single crystals. The deep research on the origin of such phenomenon will be meaningful for the further design and synthesis of such crystalline materials and understanding the structure–property relationship of nanomaterials.

According to the HRTEM (Figure 1F), which reflects the layered structure of the nano-octahedrons, and the single-crystal X-ray diffraction analysis, the selective etching mechanism was illustrated, as shown in Figure 6. Figure 6A–C shows the molecular packing of a corresponding cross section along a different direction. The selective etching of nano-octahedrons into hollow tetrahedral plates with the decrease in the pH showed that the etching speed of the two vertices at the opposite position is faster than the other four vertices and the surface. On the basis of previous investigation,[29,30] the decrease in the pH value of the suspension system along with the evaporation of water can lead to the breaking of hydrogen bonds. The phenomenon previously mentioned clearly reflects the anisotropic nature of the crystalline nanomaterials,[18,34,35] according to which the direction that etched faster should belong to the same crystal face, so that the hydrogen bond is richer than other crystal faces. In the direction perpendicular to the plane of the lamellar structure, as shown in Figure 6A, all hydrogen-bond chains of the sheet-like structure are exposed to the surface, while in the direction parallel to the porphyrin core, only part of the hydrogen bond chains are exposed (Figure 6B,C). The decrease in pH led to the break of (pyridine)N^+-H···Cl^-···H–O(H_2O)···H–N^+ (pyridine) hydrogen-bond network; then, owing to the large static repulsion among the positively charged anionic porphyrin molecules, the strong $\pi-\pi$ stacking interaction was overcome and the nanostructures dissolved (Figure 6D). The etching rate at different direction of the surface is different owing to the different density of hydrogen bonds. As a consequence, the etching speed at the direction shown in Figure 6A will be faster than that at the other two directions, resulting in the appearance of the etched hole at the corresponding two vertices, which grows larger when more hydrogen bonds are exposed owing to the dissolution of the surface molecules. Such a novel stimulus-responsive morphology modulation originating from the unique nanoeffect is very interesting and may be helpful for the construction of a more complicated nanostructure. The mechanism of pH-sensitive reversible transformation between $(H_6TPyP)^{4+}\cdot 4Cl^-$ nanocrystals and bulk single crystal was also illustrated, as shown in Figure 6. As discussed in the Experimental Section, with the decrease in pH by evaporating water, the nanocrystals gradually dissolve into $(H_6TPyP)^{4+}\cdot 4Cl^-$ molecule and then crystallize into bulk single crystals, while increase in pH by adding water again leads to the regeneration of nanostructures. Obviously, the key point is that the nanocrystals are stable at low pH, while the bulk single crystals are stable at high pH despite their same molecular composition. The only different parameter of the two crystalline materials is the size. For nanomaterials, a unique property is the surface effect.[36,37] It is well known that along with the reduction of the particle size the surface effect became stronger, which adsorbs the extra species onto the surface of the nanostructure to reduce the surface energy. In our experiment,

dx.doi.org/10.1021/jp4056544 | J. Phys. Chem. C 2013, 117, 17352–17359

owing to the surface effect, the H^+, which exists in the form of H_3O^+, was adsorbed onto the surface of the nanocrystals with the size of 250 nm to reduce the surface energy, leading to the concentration of H^+ at the surface of nanocrystals being higher than that in the suspension. However, at high pH, the number of H^+ at the surface is not large enough to break down the hydrogen bonds, rendering the nanocrystals to be stable. However, when pH increased gradually, the number of H^+ at the surface of the nanocrystals increased, which finally lead to the break of (pyridine)N^+−H···Cl^-···H−O(H_2O)···H−N^+(pyridine) hydrogen-bond networks at the surface and then deeper. However, for the bulk single crystals, the size is so large that the surface effect can be ignored, making the bulk single crystal stable at the same pH environment. As a total result, the nanocrystals gradually etched and transformed into bulk single crystals gradually. When the pH increased by adding water, hydrogen bond did not break down any more, but new ones preferred to form. In this case, the free porphyrin molecules will first nucleate on the etched nanocrystals due to the large surface effect, which led to the decrease in the concentration of free $(H_6TPyP)^{4+}\cdot 4Cl^-$ molecules in suspension and finally resulted in the dissolution of bulk single crystals owing to the shift of equilibrium. Obviously, the different surface effect between nanocrystals and bulk single crystals is actually the origin of the pH-sensitive structure transformation between nanocrystals and bulk single crystals.

CONCLUSIONS

Crystalline nano-octahedrons are easily prepared in water by self-assembling of cationic porphyrin $(H_6TPyP)^{4+}\cdot 4Cl^-$ produced through chemical reaction route in aqueous solution depending on the synergistic interactions among hydrogen-bonding, $\pi-\pi$ stacking, and ion-pairing. The separated nucleation and growth in the chemical route as well as the residue HCl are responsible for the crystallization process. Most interestingly, the unique pH-sensitive nature of the (pyridine)-N^+−H···Cl^-···H−O(H_2O)···H−N^+(pyridine) hydrogen bonds leads to the reversible transformation of nanocrystals and bulk single crystals just by adjusting the pH of the suspension by evaporating or adding water, in which the unique surface effect and anisotropic character of the nanomaterials play key role. The present result, to control the crystallinity and the unprecedented reversible transformation between nanocrystals and bulk single crystals just by tuning the pH of the synthesis process, provides a useful tool to the controlled synthesis of crystalline materials and is surely helpful for further research and application of organic nanomaterials.

ASSOCIATED CONTENT

Supporting Information

Optical microscopic image of the $(H_6TPyP)^{4+}\cdot 4Cl^-$ single crystals, molecular structure of $(H_6TPyP)^{4+}$ in the single crystal, SEM images of the self-assembled $(H_6TPyP)^{4+}\cdot 4Cl^-$ nano-octahedrons by readdition of water into the single-crystal-containing system, and crystal data and structure refinements of $(H_6TPyP)^{4+}\cdot 4Cl^-$. This material is available free of charge via the Internet at http://pubs.acs.org.

AUTHOR INFORMATION

Corresponding Author

*E-mail: jianzhuang@ustb.edu.cn.

Notes

The authors declare no competing financial interest.

ACKNOWLEDGMENTS

Financial support from the National Key Basic Research Program of China (Grant Nos. 2013CB933402 and 2012CB224801), Natural Science Foundation of China, Beijing Municipal Commission of Education, and University of Science and Technology Beijing is gratefully acknowledged.

REFERENCES

(1) Mas-Torrent, M.; Rovira, C. Role of Molecular Order and Solid-State Structure in Organic Field-Effect Transistors. *Chem. Rev.* **2011**, *111*, 4833−4856.
(2) Zhang, W.; Xiong, R.-G. Ferroelectric Metal Organic Frameworks. *Chem. Rev.* **2012**, *112*, 1163−1195.
(3) Zhang, J.-P.; Zhang, Y.-B.; Lin, J.-B.; Chen, X.-M. Metal Azolate Frameworks: From Crystal Engineering to Functional Materials. *Chem. Rev.* **2012**, *112*, 1001−1033.
(4) Li, R.; Hu, W.; Liu, Y.; Zhu, D. Micro- and Nanocrystals of Organic Semiconductors. *Acc. Chem. Res.* **2010**, *43*, 530−540.
(5) Zhao, Y. S.; Yang, W.; Xiao, D.; Sheng, X.; Yang, X.; Shuai, Z.; Luo, Y.; Yao, J. Single-Crystalline Submicrotubes from Small Organic Molecules. *J. Chem. Mater.* **2005**, *17*, 6430−6435.
(6) Lin, Z.-Q.; Sun, P.-J.; Tay, Y.-Y.; Liang, J.; Liu, Y.; Shi, N.-E.; Xie, L.-H.; Yi, M.-D.; Qian, Y.; Fan, Q.-L.; et al. Kinetically Controlled Assembly of a Spirocyclic Aromatic Hydrocarbon into Polyhedral Micro/Nanocrystals. *ACS Nano* **2012**, *6*, 5309−5319.
(7) Tao, A. R.; Huang, J.; Yang, P. Langmuir-Blodgettry of Nanocrystals and Nanowires. *Acc. Chem. Res.* **2008**, *41*, 1662−1673.
(8) Smith, A. M.; Nie, S. Semiconductor Nanocrystals: Structure, Properties, and Band Gap Engineering. *Acc. Chem. Res.* **2010**, *43*, 190−200.
(9) Zhang, Y.; Chen, P.; Jiang, L.; Hu, W.; Liu, M. Controllable Fabrication of Supramolecular Nanocoils and Nanoribbons and Their Morphology-Dependent Photoswitching. *J. Am. Chem. Soc.* **2009**, *131*, 2756−2757.
(10) Kang, L. T; Wang, Z. C; Cao, Z. W; Ma, Y.; Fu, H. B; Yao, J. N. Colloid Chemical Reaction Route to the Preparation of Nearly Monodispersed Perylene Nanoparticles: Size-Tunable Synthesis and Three-Dimensional Self-Organization. *J. Am. Chem. Soc.* **2007**, *129*, 7305−7312.
(11) Wang, T.; Jiang, J.; Liu, Y.; Li, Z.; Liu, M. Hierarchical Self-Assembly of Bolaamphiphiles with a Hybrid Spacer and L-Glutamic Acid Headgroup: pH- and Surface-Triggered Hydrogels, Vesicles, Nanofibers, and Nanotubes. *Langmuir* **2010**, *26*, 18694−18700.
(12) Rodler, F.; Linders, J.; Fenske, T.; Rehm, T.; Mayer, C.; Schmuck, C. pH-Switchable Vesicles from a Serine-Derived Guanidiniocarbonyl Pyrrole Carboxylate Zwitterion in DMSO. *Angew. Chem., Int. Ed.* **2010**, *49*, 8747−8750.
(13) Nieuwenhuizen, M. M. L.; de Greef, T. F. A.; van der Bruggen, R. L. J.; Paulusse, J. M. J.; Appel, W. P. J.; Smulders, M. M. J.; Sijbesma, R. P.; Meijer, E. W. Self-Assembly of Ureido-Pyrimidinone Dimers into One-Dimensional Stacks by Lateral Hydrogen Bonding. *Chem.—Eur. J.* **2010**, *16*, 1601−1612.
(14) Gao, Y.; Zhang, X.; Ma, C.; Li, X.; Jiang, J. Morphology-Controlled Self-Assembled Nanostructures of 5,15-Di[4-(5-acetylsulfanylpentyloxy)phenyl]porphyrin Derivatives. Effect of Metal-Ligand Coordination Bonding on Tuning the Intermolecular Interaction. *J. Am. Chem. Soc.* **2008**, *130*, 17044−17052.
(15) Lu, G.; Zhang, X.; Cai, X.; Jiang, J. Tuning the Morphology of Self-Assembled Nanostructures of Amphiphilic Tetra(p-hydroxyphenyl)porphyrins with Hydrogen Bonding and Metal−Ligand Coordination Bonding. *J. Mater. Chem.* **2009**, *19*, 2417−2424.
(16) Ma, P.; Chen, Y.; Bian, Y.; Jiang, J. Morphology Controlled Surface-Assisted Self-Assembled Microtube Junctions and Dendrites of Metal Free Porphyrin-Based Semiconductor. *Langmuir* **2010**, *26*, 3678−3684.

(17) Wang, Q.; Chen, Y.; Ma, P.; Lu, J.; Zhang, X.; Jiang, J. Morphology and Chirality Controlled Self-assembled Nanostructures of Porphyrin−pentapeptide Conjugate: Effect of the Peptide Secondary Conformation. *J. Mater. Chem.* **2011**, *21*, 8057−8065.
(18) Sun, W.; Wang, H. L.; Qi, D. D.; Wang, L.; Wang, K.; Kan, J. L.; Li, W, J.; Chen, Y. L.; Jiang, J. Z. 5,10,15,20-Tetra(4-pyridyl)-porphyrinato Zinc Coordination Polymeric Particles with Different Shapes and Luminescent Properties. *CrystEngComm* **2012**, *14*, 7780−7786.
(19) Lu, G.; Chen, Y..; Zhang, Y.; Bao, M.; Bian, Y.; Li, X.; Jiang, J. Morphology Controlled Self-Assembled Nanostructures of Sandwich Mixed (Phthalocyaninato)(Porphyrinato) Europium Triple-Deckers. Effect of Hydrogen Bonding on Tuning the Intermolecular Interaction. *J. Am. Chem. Soc.* **2008**, *130*, 11623−11630.
(20) Ma, P.; Chen, Y.; Bian, Y.; Jiang, J. Synthesis, Characterization and OFET Properties of Amphiphilic Mixed (Phthalocyaninato)-(porphyrinato)europium(III) Complexes. *Eur. J. Inorg. Chem.* **2009**, 954−960.
(21) Lu, G.; Ou, Z.; Jiang, J.; Bian, Y. Nanoscale Hollow Spheres of an Amphiphilic Mixed (Phthalocyaninato)(porphyrinato)europium Double-Decker Complex. *Eur. J. Inorg. Chem.* **2010**, 753−757.
(22) Lu, J.; Wu, L.; Jiang, J.; Zhang, X. Helical Nanostructures of an Optically Active Metal-Free Porphyrin with Four Optically Active Binaphthyl Moieties: Effect of Metal−Ligand Coordination on the Morphology. *Eur. J. Inorg. Chem.* **2010**, 4000−4008.
(23) Zhang, X.; Wang, Q.; Wu, L.; Lv, W.; Lu, J.; Bian, Y.; Jiang, J. Organic Nanostructures with Controllable Morphology Fabricated from Mixed (Phthalocyaninato)(porphyrinato) Europium Double-Decker Complexes. *J. Phys. Chem. B* **2010**, *114*, 1233−1240.
(24) Blessing, R. H. An Empirical Correction for Absorption Anisotropy. *Acta Crystallogr.* **1995**, *A51*, 33−38.
(25) *SHELXL Reference Manual*, version 5.1; Bruker Analytical X-Ray Systems: Madison, WI, 1997.
(26) Luca, G. D.; Romeo, A.; Scolaro, L. M. Role of Counteranions in Acid-Induced Aggregation of Isomeric Tetrapyridylporphyrins in Organic Solvents. *J. Phys. Chem. B.* **2005**, *109*, 7149−7158.
(27) Huang, C.; Li, Y.; Song, Y.; Li, Y.; Liu, H.; Zhu, D. Ordered Nanosphere Alignment of Porphyrin for the Improvement of Nonlinear Optical Properties. *Adv. Mater.* **2010**, *22*, 3532−3536.
(28) Arai, Y.; Segawa, H. Cl^- Complexation Induced H- and J-Aggregation of *meso*-Tetrakis(4-sulfonatothienyl)porphyrin Diacid in Aqueous Solution. *J. Phys. Chem. B* **2011**, *115*, 7773−7780.
(29) Bian, Y.; Jiang, J.; Tao, Y.; Choi, M. T. M.; Li, R.; Ng, A. C. H.; Zhu, P.; Pan, N.; Mak, T. C. W.; Ng, D. K. P.; et al. Tuning the Valence of the Cerium Center in (Na)phthalocyaninato and Porphyrinato Cerium Double-Deckers by Changing the Nature of the Tetrapyrrole Ligands. *J. Am. Chem. Soc.* **2003**, *125*, 12257−12267.
(30) Fan, J.; Fang, G.; Wang, X.; Zeng, F.; Xiang, Y.; Wu, S. Targeted Anticancer Prodrug with Mesoporous Silica Nanoparticles as Vehicles. *Nanotechnology* **2011**, *22*, 455102.
(31) Li, R.; Zhang, Y.; Zhou, Y.; Dong, S.; Zhang, X.; Bian, Y.; Jiang, J. H_2O-Involved Hydrogen Bonds in Pseudo-Double-Decker Supramolecular Structure of 1,8,15,22-Tetrasubstituted Phthalocyaninato Zinc Complex. *Cryst. Growth Des.* **2008**, *8*, 4454−4459.
(32) Wang, R.; Li, R.; Li, Y.; Zhang, X.; Zhu, P.; Lo, P. C.; Ng, D. K. P.; Pan, N.; Kobayashi, N.; Jiang, J.; et al. Controlling the Nature of Mixed (Phthalocyaninato)(porphyrinato) Rare- Earth(iii) Double-Decker Complexes: The Effects of Nonperipheral Alkoxy Substitution of the Phthalocyanine Ligand. *Chem.—Eur. J.* **2006**, *12*, 1475−1485.
(33) Wang, D.; Su, Y.; Jin, C.; Zhu, B.; Pang, Y.; Zhu, L.; Liu, J.; Tu, C.; Yan, D.; Zhu, X. Supramolecular Copolymer Micelles Based on the Complementary Multiple Hydrogen Bonds of Nucleobases for Drug Delivery. *Biomacromolecules* **2011**, *12*, 1370−1379.
(34) Meng, F.; Morin, S. A.; Forticaux, A.; Jin, S. Screw Dislocation Driven Growth of Nanomaterials. *Acc. Chem. Res.* **2013**, *46*, 1616−1626.
(35) Huang, Y.; Wu, L.; Chen, X.; Bai, P.; Kim, D.-H. Synthesis of Anisotropic Concave Gold Nanocuboids with Distinctive Plasmonic Properties. *Chem. Mater.* **2013**, *25*, 2470−2475.
(36) Pan, N.; Wang, X.; Li, M.; Li, F.; Hou, J. G. Strong Surface Effect on Cathodoluminescence of an Individual Tapered ZnO Nanorod. *J. Phys. Chem. C* **2007**, *111*, 17265−17267.
(37) Gursky, J. A.; Blough, S. D.; Luna, C.; Gomez, C.; Luevano, A. N.; Gardner, E. A. Particle-Particle Interactions between Layered Double Hydroxide Nanoparticles. *J. Am. Chem. Soc.* **2006**, *128*, 8376−8377.